Banos, A., Hallam, K. R., & Scott, T. B. (2019). Corrosion of uranium in liquid water under contained conditions with a headspace deuterium overpressure. Part 2: The ternary U + $H_2O_{(l)}$ + D_2 system. *Corrosion Science*, *152*, 261-270. https://doi.org/10.1016/j.corsci.2019.02.016

Corrosion Science 152 (2019) 261–270

Contents lists available at ScienceDirect

Corrosion Science

journal homepage: www.elsevier.com/locate/corsci

Corrosion of uranium in liquid water under contained conditions with a headspace deuterium overpressure. Part 2: The ternary U + $H_2O_{(l)}$ + D_2 system

A. Banos*, K.R. Hallam, T.B. Scott

University of Bristol, Interface Analysis Centre, School of Physics, HH Wills Physics Laboratory, Tyndall Avenue, Bristol, BS8 1TL, United Kingdom

ARTICLE INFO

Keywords:
Uranium
Water corrosion
Bulk-UH_3
Threshold pressure
FIB

ABSTRACT

The reaction of unirradiated-U with liquid water under deuterium overpressure was studied by conducting nine separate reactions at different temperatures. Post-corrosion examination of the surfaces was conducted using FIB, SIMS and XRD. Measurements of the reacting-water pH and sample degassing were made after the experiments were stopped. Isotopic labelling allowed better investigation of the mechanisms occurring in this system. The analyses showed that bulk-UH3 forms at the metal-oxide interface. The observed gas evolution reduction in the headspace was attributed to gas suppression of hydrogen generated through oxidation, and **not** D2 gas migration through the water. This suppression facilitates UH3 formation.

1. Introduction

There are legacy ponds and silos at Sellafield, accommodating most all historically generated British intermediate level waste (ILW) containing uranium metal. These facilities which were initially meant for interim storage of material waiting to be reprocessed are now decades old and there is an increasing urgency for this material to be safely retrieved and prepared for long-term storage and disposal. ILW is mainly comprised of activated and contaminated metals and materials, such as reactor components, fuel-cladding and conditioned fuel parts [1]. This waste is stored either in containers immersed in water (sludge ponds) or as unsorted debris piles within containment cells e.g. silos, where both vapour and liquid water are abundant [2]. Uranium metal would initially have been found in significant quantities in this ILW. Thus, uranium and uranium-containing components have been exposed to differing corrosion conditions over prolonged periods, under water-immersed and/or contained storage conditions. Uranium will readily react with water to produce uranium dioxide (UO_2) and hydrogen gas (H_2) (Eq. 1). If H_2 does not escape to dilute in the atmosphere but instead remains trapped in the near vicinity of the metal, a complex ternary U-H_2O-H_2 reaction system will establish itself. If H_2 build up in high concentrations it will react with uranium to form uranium hydride (UH_3) (Eq. 2).

$$U_{(s)} + 2H_2O_{(l)} \rightarrow UO_{2(s)} + 2H_{2(g)} \quad (1)$$

$$2U_{(s)} + 3H_{2(g)} \rightarrow 2UH_{3(s)} \quad (2)$$

UH_3 is regarded as being unstable in air and pyrophoric under certain conditions (e.g. high surface area and mass) [3,4]. Thus, its formation is undesirable and generates serious safety and technical challenges for the nuclear industry. In the literature there is a controversy over whether UH_3 can form, concurrent with UO_2, as part of the uranium-water reaction [5–17] or not [18–21]. In reality, UH_3 formation in such a system depends on a number of parameters such as whether it is an enclosed/sealed system [5,9,16] or not [7,19], the temperature of the reaction [5], or the physical state of the reacting water (solid, liquid, vapour/steam) [5], etc.

In previous works [22], we have examined the corrosion of uranium under water immersion conditions in sealed cells in which the headspace volume was initially evacuated. From the analysis, it was confirmed that along with UO_2 formation, UH_3 also forms as a solid product of corrosion. It was also observed that above a certain headspace pressure of hydrogen, the rate of continuing gas evolution into the headspace, arising from corrosion, was significantly decreased. This was ascribed to the onset of substantial UH_3 formation on the reacted samples and was evidenced by combining the data arising from post-reaction examination of the reacted surface, with reaction rate behaviour (through H_2 evolution). In this current work, we have made an experimental attempt to monitor the mechanisms of reaction as well as reaction rates in the earlier stages of corrosion. By introducing deuterium (D_2) at a known pressure into the system gas space instead of

* Corresponding author.
E-mail address: antonis.banos@bristol.ac.uk (A. Banos).

https://doi.org/10.1016/j.corsci.2019.02.016
Received 18 September 2018; Received in revised form 13 February 2019; Accepted 14 February 2019
Available online 19 February 2019

hydrogen, the isotopic-labelling could be used to track the movement of D_2 within the system. This isotopic spiking was hoped to better elucidate the mechanisms for corrosion within the ternary system.

There is only a very limited amount of published experimental work examining the ternary uranium-water-hydrogen corrosion system, especially under water-immersed conditions. Baker et al. [23] examined the effect of hydrogen overpressure on a water-immersed uranium sample and found no significant effect of this pressure to the corrosion rate or the arising reaction products, even up to 6 atm (or ~609750 Pa) gas pressure. However, Baker adopted an experimental set-up where the sealed reaction system was periodically opened for thermogravimetric analysis to be performed. Thus, the system was kept under sealed conditions for only a limited amount of time. Furthermore, this work did not provide any information about the headspace volume, mass of sample and volume of water utilised, which for an extended time period, could immensely affect the kinetics and products of the reaction [9]. In the same work, other bystander gases such as N_2 (1013.3 mbar or 101325 Pa) and CO_2 (~71 to 2027 mbar or 7100–202700 Pa) were introduced in the headspace, with the former showing no effect on the rate and the latter showing a substantial slowing of the corrosion rate to as much as half the original value. For CO_2, formation of carbonate ions on the oxide surface was suggested as responsible for diffusion at blocking of H_2 to reach the gas headspace. In our previous work [22], it was inferred that after the headspace pressure reached a critical value, (which specifically for the parameters of our systems was calculated in the 500-mbar range), the rate of H_2 gas evolution became suppressed and/or water - hydrogen exchange occurred in the system, leading to UH_3 formation [22]. Above the 'threshold pressure', suppression of H_2 gas release out from the outermost oxide surface, through the water and into the headspace, was considered highly possible, since water molecules chemisorb on the available surface sites blocking outwards diffusion of hydrogen, generated at the metal-oxide interface. Additionally, above the 'threshold pressure', hydrogen concentration in the headspace will be equal to or higher than the hydrogen concentration at the metal-oxide interface, thereby promoting UH_3 formation. The opposite process, which was the migration of the gas from the headspace into water and eventually to the metal surface was regarded as thermodynamically less favoured. This is because chemisorbed water will inhibit further chemisorption and dissociation of H_2 at the oxide surface, by blocking all available sorption sites [24]. Of course, strain and disruption on the oxide surface caused either by an originally strained metal surface [25] or by volume expansion (loss of coherence), would lead to more available and direct diffusion pathways for hydrogen to reach the metal and react with the uranium. Hence, this process cannot be ruled out. Based on the previous success of using isotopic waters to study metal/hydride corrosion [26], isotopic labelling of the starting headspace gas was considered a viable experimental option for better investigating the mechanistic processes occurring in this ternary corrosion system. Thus, in this work, the experimental set-up of our former work [22] was repeated, but this time D_2 gas of known starting pressure was introduced to the free headspace volume from the outset of the experiment. Maintaining the same reaction conditions, experimental procedure and methods of examination was imperative to secure reliable and comparable conclusions with respect to the mechanisms driving the ternary system, while also verifying the previously reported findings of [22].

2. Materials and experimental methods

2.1. Sample preparation

A total of nine samples were prepared for this work, all originating from the same batch of as-cast Magnox-U metal. Extensive description of the metal was provided in previous publications [22,27–29]. Table 1 integrates the initial sample parameters for the corrosion experiments. The letter 'W' was used to designate the liquid reactant, 'D' was used to denote the gas reactant (D_2) filling the headspace volume; the accompanying numbers denote the temperature of the reaction and the ending letter denote the headspace pressure, with 'L' denoting low, 'M' medium and 'H' high pressure of D_2, respectively. Low D_2 pressure was considered as an initially established headspace pressure in the 250-mbar range, medium in the 500-mbar range and high in the 750-mbar range. Thus, for a sample that was reacted with water at 45 °C, with high D_2 headspace pressure, the denotation WD45H was used.

Table 1
Preliminary parameters (weight & surface area) of the samples.

Sample	Mass (g)	Surface area (cm^2)
WD25L	1.58	1.38
WD25M	3.02	2.35
WD45L	4.43	3.54
WD45M	5.1	3.7
WD45H	1.93	1.86
WD55L	4.44	3.68
WD55M	1.35	1.35
WD55H	4.5	3.59
WD70M	4.8	3.55

2.2. Reactant water

The same freeze-vacuum-melt process described in [22] was followed for the preparation of the reaction water used in this work. The purpose of this preparation was to remove dissolved oxygen from the water, which would complicate determination of the reaction mechanisms. It is recognised that deliberate alteration of pH, 'oxygen poisoning' and/or introduction of salts would have altered the aqueous corrosion rates, but understanding these interactions was not the aim of the experiment.

2.3. Headspace gas (D_2)

The gas used to fill the headspace volume for the start of each reaction was 99.99% pure D_2, provided by BOC gases. The gas was stored in a $LaNi_5$ bed to reduce gas impurities and was introduced into the volume by connecting the reaction pot cell to the gas control rig (and associated pressure controller).

2.4. Experimental apparatus

The reaction pot cells constructed for the experimental work of [22] were also used for this work. More extensive description of the set-up can be found in [22].

2.5. Experimental method

The experimental procedure described in [22] was also followed in the present work, with one additional step included in the process. Immediately after the third stage of the freeze-vacuum-melt process and evacuation, the cell was opened and the sample was positioned on top of the solidified water (ice) in the crucible. The cell was then sealed and immersed in liquid N_2 to be evacuated for a final time. After suitable vacuum was reached ($\leq 1 \times 10^{-6}$ mbar), the set-up was connected to a data logging system for measuring changes in cell pressure and temperature. The cell was subsequently placed in an oven for heating to the desired reaction temperature. The pressure was then closely monitored to determine when the contained ice was fully melted, and the set-up was then briefly withdrawn from the oven, connected to a gas control rig and D_2 was admitted at a set pressure. If we consider the 'threshold' pressure value always close to the ~500 mbar range [22], then for higher reaction temperature less initial D_2 pressure was needed to be introduced to the cell volume to achieve that value. The average time

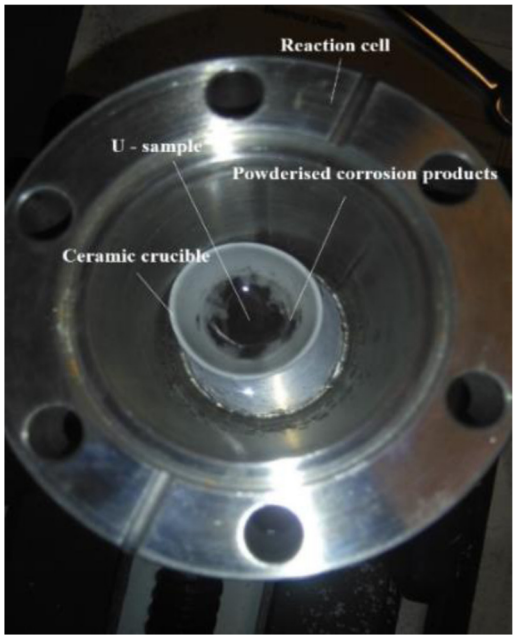

Fig. 1. An opened experimental cell immediately after reaction completion. The sample was flaked-off and powderised, with clearly observable (black) reaction products, spread across the base of the ceramic crucible containing the water. Figure reproduced from [26].

needed for D_2 admission was approximately 2 min. The measured pressure after D_2 filling, was considered to represent the water vapour pressure prior to D_2 admission plus the admitted D_2 gas. The cell was then quickly placed back into the oven. An overall gas pressure in the range of 500 mbar (medium pressure) at the desired reaction temperature was targeted for all the initial experimental runs. High (˜750 mbar) and low (˜250 mbar) D_2 pressures were admitted in the subsequent experiments. In all cases the reaction was halted by opening the cell and carefully retrieving the sample (in air) from the ceramic crucible containing the water. Partial mass loss was inevitable at this stage of the process when significant thicknesses of corrosion products had accumulated (Fig. 1). The sample was left in laboratory air to dry for 2–3 min s and placed in an inert atmosphere (Ar-filled glovebox), awaiting post-examination and analysis.

2.6. Post-reaction examination

We ensured that our experimental setup was identical to prior experiments [22], since direct comparison or results was desired. The protocol for post-reaction analysis was maintained for the same reason. Thus, focused ion beam (FIB) milling and sectioning, secondary ion mass spectrometry (SIMS), X-ray diffraction (XRD) and temperature-programmed desorption (TPD) combined with residual gas analysis (RGA) were the methods utilised for sample examination.

2.7. Assumptions

The assumptions identified in previous experiments [22] were adopted for this work. Notably, α-U was assumed to be the only phase on the sample, ignoring the fact that Magnox natural-U has a carbon content of ˜1000 carbides. mm^{-2}.

For determining the U oxidation rate, only gaseous H_2 and solid uranium dioxide (UO_2) were assumed to be produced according to Eq. 1. UH_3 which may be produced though Eq. 2 was deliberately excluded from our calculations. Subsequently any observed mismatch between the oxidation rates derived by different methods (H_2 generation versus direct oxide thickness measurements), could imply UH_3 formation within the system in addition to UO_2.

Other significant assumptions were that (1) no significant reaction is taking place on the uranium surface during the time needed to complete D_2 gas filling and reach the desired reaction temperature; (2) negligible amounts of D_2 gas, (in comparison to the overall gas pressure) is dissolved in the reaction water. For the former assumption, this short preparation period is regarded as negligible when compared to the total reaction time of each system (on the order of 100's of hours). For the latter assumption, blank tests using identical conditions but without a sample in the cell (not shown here) demonstrated that after initial equilibrium was reached, the headspace gas pressure remained constant for 100's of hours.

3. Results

Not all specimens were examined with all techniques/methods, with certain analysis on later samples being deliberately skipped to minimise cumulative damage.

3.1. Reaction rate determinations via gas generation

Sample reaction rates were calculated using the recorded gas pressure changes with time. Pressure change was ascribed to H_2 generation from water oxidation, through Eq. 1. The moles of H_2 generated were converted, (through Eq. 1) to moles of reacted U per unit area with time ($mgU.\ cm^{-2}.\ h^{-1}$). Fig. 2 illustrates a representative reaction plot for a sample corroding at 70 °C under a starting D_2 pressure of 448 mbar for 516 h. Plots at other temperatures displayed similar reaction profiles.

Multiple reaction rate regimes may be observed from the graph (Fig. 2). The various reaction rate regimes, as derived from the graphs, are displayed in Table 2 (middle columns). The average reaction rate, shown in the last column of Table 2, was derived from the average of: (a) the average values of differential rates derived every hour and (b) the rate which was derived from the total U mass consumption, per unit area, divided by the total reaction time. The table also includes the initial D_2 pressure introduced to the cell at the start of the reaction.

3.1.1. Reaction rate line behaviour

For samples reacted at 25 and 45 °C reactions (not shown here), the recorded samples exhibited two poorly discriminated rate regimes, with the first being slightly higher than the other indicating more rapid initial oxidation. For samples corroded at 55 and 70 °C, an example of which is shown in Fig. 2, the recorded reaction profiles were very

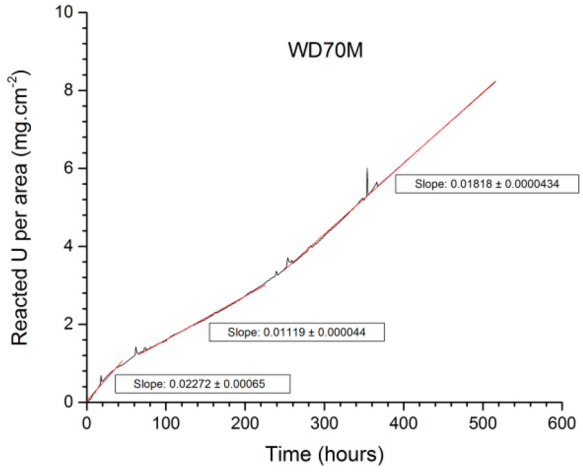

Fig. 2. Corrosion progress of uranium immersed in water with D2 overpressure for WD70 M sample. The rate was derived from pressure changes (ascribed to H2 generation), converted to milligrams of reacted U per unit area, over time. Figure reproduced from [26].

Table 2
The reaction rate regimes derived from for each experimental condition, for the ternary uranium-liquid water-deuterium system.

Sample	D_2 pressure (mbar)*	Time of reaction (hours)	Reaction Rate 1st regime (mgU. cm^{-2}. h^{-1})	Reaction Rate 2nd regime (mgU. cm^{-2}. h^{-1})	Reaction Rate 3rd regime (mgU. cm^{-2}. h^{-1})	Average Reaction Rate (mgU. cm^{-2}. h^{1})
WD25L	$222.3_{(28.1\ °C)}$	1047.4	0.0074 ± 0.0006	0.0067 ± 0.0003	0.0017 ± 0.0003	0.0041
WD25M	$551.7_{(26.6\ °C)}$	1091	n/a	0.0038 ± 0.0001	0.0033 ± 0.00004	0.003
WD45L	$240_{(48.8\ °C)}$	1567.4	0.0049 ± 0.0001	0.0125 ± 0.0003	0.0297 ± 0.00007	0.0181
WD45M	$447.8_{(44.2\ °C)}$	775	n/a	0.0023 ± 0.0002	n/a	0.0023
WD45H	$734.2_{(45.6\ °)}$	1639	0.0038 ± 0.0005	0.0126 ± 0.0004	0.0206 ± 0.0002	0.0148
WD55L	$151_{(56.3\ °C)}$	1566	0.0447 ± 0.0003	0.0379 ± 0.0002	0.0546 ± 0.00002	0.044
WD55M	$416_{(54.5\ °C)}$	1075	n/a	0.0381 ± 0.0007	0.0496 ± 0.00008	0.044
WD55H	$728_{(54.2\ °C)}$	1092.3	0.0255 ± 0.0007	0.0169 ± 0.0007	0.0182 ± 0.0001	0.017
WD70M	$447.9_{(69.8\ °C)}$	516	0.0227 ± 0.0007	0.0112 ± 0.0007	0.0182 ± 0.00004	0.016

* The overall pressure on the headspace includes the D_2 pressure at the temperature of reaction, added to the pressure of water vapour saturation.

similar, exhibiting an (1) initial linear/parabolic rate of gas generation followed by (2) a linear rate of gas production which eventually switches to (3) constant gas production but at a higher linear rate.

3.1.2. Average rate - Comparison to a U + H_2O reaction system

The average reaction rate values for all temperatures (Table 2), determined from measured headspace H_2 increases, were significantly lower in comparison to those determined from a directly comparable set of experiments exploring the binary U + H_2O system [22]. For the 25 °C regime, the average rate was 2 to 3 times slower in comparison to the U + H_2O system [22]. At 45 °C, recorded rates were still lower than the binary system, but with final reaction rate periods (regime 3) being directly comparable. At 55 °C, the overall corrosion rate was 28–45 % lower than for the binary system. Finally, at 70 °C, the average corrosion rate was up to ~90% slower than the equivalent binary system [22]. Thus, it can be inferred that the initial headspace gas overpressure had a significant effect on the rate of H_2 generation into the headspace. This is consistent with the observation made in [22] where the observed reaction rates were observed to switch to a slower rate regime once a critical 'threshold pressure' had been reached in the cell headspace.

3.1.3. Effect of D_2 overpressure

Based on the previous study of the binary system [22], where a 'threshold pressure' between 450 - 550-mbar was observed to alter the gas generation rate from U oxidation, the current experiments deliberately selected starting headspace pressures above, at and below this observed threshold. Sample reaction temperatures of 45 °C and 55 °C were arbitrarily chosen, with an additional run was also conducted for the 25 °C regime, with the overall pressure lying below the 0.5 bar range (sample WD25 L).

Compared to the other samples reacting at 25 °C that had a starting headspace pressure of 500 mbar, the average reaction rate measured for WD25 L was higher, indicating that the threshold suppression remained true. At 45 °C, the average rate was also higher for sample WD45 L (starting below threshold pressure) in comparison to WD45H (starting above threshold pressure). Sample WD45 M exhibited a more complex rate profile with a surprisingly low average reaction rate. At 55 °C, the samples starting below and at the threshold pressure (WD55 L and WD55 M) yielded similar average rates. As expected, sample WD55 L exhibited a higher reaction rate in the last 500 h of reaction, with a headspace pressure remaining below the threshold pressure (Table 2). Sample WD55H which had a starting headspace pressure above 500 mbar exhibited significantly lower reaction rates than WD55 M or WD55 L. Overall, a trend was observed for declining gas generation rates from U oxidation with increasing headspace pressure. This implies either (i) oxidation rates are supressed by the gas overpressure or (ii) oxidation rates are not supressed but instead a proportion of the hydrogen released is consumed by hydride (UH_3) formation.

3.2. Oxide thickness layer calculations - Rate determination

An alternative method for determining the U oxidation rate was via direct measurement of corrosion layer thickness at the end of each experiment. This was achieved using FIB to make several cross-sectional cuts on each sample and directly measure the thickness of the corrosion layer.

At the time of measurement this layer was assumed to be exclusively UO_2. The derived average of multiple thickness measurements was then used to calculate an overall reaction rate for each sample that could be directly compared to the rate determined by gas generation. If for any sample, the reaction rate derived from corrosion layer thickness measurements was significantly higher than that derived from gas generation, it is highly probable that UH_3 (in addition to UO_2) has formed at the metal-oxide interface. Even though both these corrosion products, UO_2 and UH_3, have a very similar density, the latter will grow in thickness without releasing any hydrogen into the gas phase (Eq. 2). Thus, if a hydride layer is inadvertently assigned to UO_2 formation this would lead to an overestimation of the oxidation rate, in comparison to the rate derived from H_2 evolution. Additionally, if UH_3 is formed it could potentially be identified through physical observation of the interface, though as shown in [22], this is very challenging, especially on heavily corroded samples where the accumulated corrosion layer is substantial.

Fig. 3 illustrates an example cross-sectional cut into a corroded U surface (sample WD70 M). From examination of the sample cross-sections (not all displayed) it could be inferred that, for the surfaces reacted at lower temperatures, the oxide is better adhered and less porous, whilst samples experiencing higher reaction temperatures exhibited delamination within the corrosion layer, with a commensurate increase in porosity. For some of these high temperature, heavily corroded samples, a change in the physical appearance of the corrosion layer was observed when approaching the metal-oxide interface (Fig. 3). It was not clear if this apparent change in morphology corresponded with the presence of UH_3 or freshly formed UO_2 exhibiting a different texture.

Comparison of the rates derived from oxide thickness measurements versus gas evolution indicates substantial differences. Table 3 displays the comparative data for each sample. In all cases, the rate derived from the thickness of the corrosion layer was higher than that derived from H_2 evolution. In extremis, the rate derived from corrosion layer thickness measurements (ascribed to UO_2) for sample WD70 M was ~5.5 times greater than derived from gas evolution. Only for sample WD55 M were the derived rates from the two methods approximately comparable.

The consistently higher reaction rates derived from oxide thickness determinations strongly implies that UO_2 was not the only corrosion product being produced from metal corrosion. However, the FIB sections could not provide direct or definitive evidence of UH_3 formation.

Similar results, though not so pronounced, were obtained from

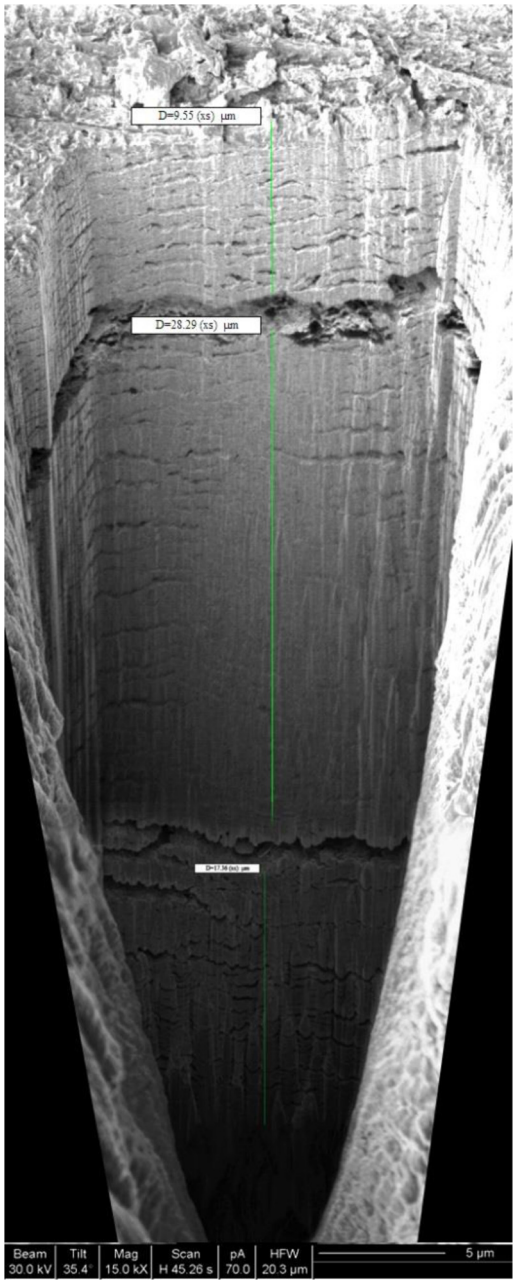

Fig. 3. Focused ion beam (FIB) milling image showing the cross-sectional view of WD70 M sample. Multiple images were produced and stitched together to demonstrate the thickness of the layer. In an effort to show the oxide on the cross-section, the periphery of the cut was inevitably saturated. Figure reproduced from [26].

analyses of samples from [22]. Three processes may be invoked as potential causes for the observed difference between the determined reaction rates for each sample. The most probable cause for this difference may be ascribed to UH_3 formation, according to Eq. 2. Less likely, is that the 'missing' hydrogen is incorporated within hydroxide phases at the oxide surface, which could be verified by SIMS and/or XRD analysis. The final option is that the hydrogen could be dissolved in the reaction water. This option may be substantially discounted considering the extremely limited reported solubility of hydrogen in water [30]. This could be confirmed by post-reaction analysis of the reaction waters.

Table 3
Oxide thickness vs H_2 generation derived rate for the ternary reaction systems.

Sample	Corrosion layer thickness (µm)	Reaction rate derived from average corrosion layer thickness measurements (ascribed to UO_2) (mgU. cm^{-2}. h^{-1})	Reaction rate derived from H_2 generation (mgU. cm^{-2}. h^{-1})
WD25M	6.36	0.0056	0.003
WD45L	71.23	0.0439	0.0181
WD45M	2.71	0.0034	0.0023
WD45H	64.05	0.0378	0.0148
WD55L	86.24	0.0533	0.044
WD55M	52.44	0.0472	0.044
WD55H	60.39	0.0535	0.017
WD70M	47.04	0.0882	0.016

3.3. pH analysis of arising reaction waters

The reaction water of seven out of nine samples was measured immediately after the reaction was ceased and the cell was opened to air. By comparing the difference in measured pH for each sample pre- and post-reaction, the concentration of H^+ could be calculated. This concentration was ascribed in totality to hydrogen generated from the oxidation of uranium (even though other entities such as dissolved UO_2 or CO_2 would contribute to the pH drop) which was converted to moles of H_2. Through the ideal gas law, moles of H_2 dissolved in the water, could then be converted to an equivalent H_2 gas pressure if it had instead entered the headspace as gas (assuming complete release). Table 4 displays the results from pH analysis, showing that in each experiment the reaction waters showed a drop in pH. This implies that some hydrogen had dissolved in the water, which was not unexpected since prior to experiment it was purged of all dissolved gases by the preparatory vacuum-freeze-thaw process. However, the calculated mass of hydrogen (moles) in each case would contribute an insignificant increase in the overall headspace pressure if it were degassed from the water. Thus, it can be assumed that dissolved gas, accounted for only an extremely limited amount of the free hydrogen in the system and therefore was an insubstantial storage sink compared to the gaseous or solid phases.

3.4. SIMS analysis of the reacted samples

SIMS analysis allowed chemical identification of the corrosion layer composition, starting from the outermost layers and progressively moving deeper towards the metal-oxide interface, through reactive ion-sputtering. Mass spectrum analysis was conducted on the surface of each sample prior to any targeted depth profiling.

Fig. 4 illustrates an example mass spectrum recorded from sample WD70 M. Hydrides and/or deuterides are indicated, with complex $UOCHD^+$ ion clusters and associated carbide-nitride-oxygen clusters also identified alongside uranium dioxide (from UO^+ and $UO_2{}^+$ clusters) which dominated the sample surface. Depth profiling combined with literature reports on previous similar SIMS experiments were used to resolve isobaric interferences in the recorded mass spectra. Formation of hydroxides and carbide-hydroxide phases/clusters, as part of water corrosion, have been previously reported by Totemeier et al. [31] and Harker [32]. Fig. 5 illustrates representative mass ion depth profiles for each system.

Deuteride, hydride and hydroxide ion clusters provided a strong indication that the outermost surface of the samples was hydrated i.e. had both physi- and chemisorbed water. This was most prominently evidenced by the appearance of ion clusters ascribed to arise from hydroxide phases such as $UO_2H_3{}^+$ ion clusters. However, the ion cluster yield and thickness of these hydrated layers were limited in their extent, implying that only the outermost surfaces (< 1 µm) were rich in hydroxide and higher oxide phases of U. The contribution of these phases

Table 4
Reaction water pH measurements and H_2 concentration calculation (as pressure increase if in the gas phase), for all ternary system experiments.

Sample	pH of water at average temperature of reaction*	pH of reactant water at average temperature of reaction	Difference in concentration of H^+ between original and reactant water (mol/lt)**	Difference in H_2 in reactant water (mmol)***	Working/ reaction volume (cm^3)****	Pressure increase if excess H_2 diffused out to the gas phase (mbar)
WD25L	6.83	6.62	9.31E-08	1.86E-07	84.81	0.00005
WD25M	n/a	Not measured	n/a	n/a	n/a	n/a
WD45L	6.53	5.91	9.45E-07	1.89E-06	84.63	0.0006
WD45M	n/a	Not measured	n/a	n/a	n/a	n/a
WD45H	6.53	6.22	3.13E-07	6.26E-07	84.77	0.0002
WD55L	6.44	5.87	9.78E-07	1.95E-06	84.62	0.0006
WD55M	6.44	5.91	8.71E-07	1.74E-06	180.45	0.0003
WD55H	6.44	6.13	3.75E-07	7.5E-07	80.75	0.0003
WD70M	6.29	5.7	1.49E-06	2.97E-06	80.73	0.001

* pH at 25.2 °C, 6.86. Linear extrapolation to the temperature of reaction and thus approximate value.
** Volume of water = 4 ml.
*** If all excess H^+ coupled to form H_2.
**** Inconsiderable change in the working volume due to sample's volume expansion and liquid water consumption.

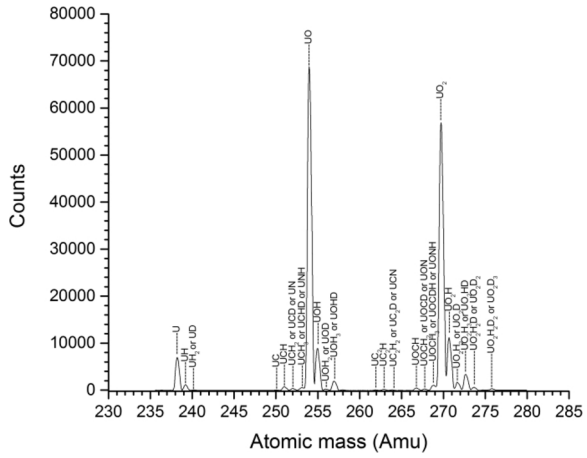

Fig. 4. Post-reaction mass spectrum analysis (230–280 Amu) for sample WD70 M. Hydrides and/or deuterides, hydroxides, uranium-oxide-deuterium-hydrogen complex phases, carbide-nitride-oxygen-deuterium clusters along with oxides can be seen in the spectrum. Figure reproduced from [26].

to the observed headspace H_2 deficiency would therefore be insignificant. The appearance of the UO_2D_3 ion cluster (276 Amu) in the outer layers of the oxide surface (Fig. 5a) indicated that some deuterium from the gas phase had managed to reach the surface of the sample. This could imply either continuous exchange between the reaction water and D_2 gas or initial interaction of this gas with the water immediately after admission, before initial thermodynamic equilibrium is reached in the system. The latter appears to be a more probable scenario since blank $H_2O_{(l)}$ + D_2 tests yielded constant gas pressure in the headspace over many 100's of hours.

Previous studies have used SIMS analysis to provide definitive confirmation of hydride formation on U metal surfaces [27–29]. In the current work, it was expected that evidence for hydride formation would be expressed in the SIMS depth profiles as a 'spike' in the recorded UH^+ and UH_2^+ (or UD^+) ion cluster yields, close to the metal-oxide interface. This behaviour was clearly observed in at least five of the nine samples. The UH^+ and UH_2^+ (or UD^+) intensity signals at 239 and 240 Amu respectively, yielded almost identical intensity profiles for the majority of depth profiles (Figs. 5a & b), indicating hydride formation at the metal oxide interface. However, it was not possible to make a clear distinction between UH_3 and UD_3 formation since the line profile at 240 Amu could equally be assigned to UH_2 or UD. This could either imply that the mass peak recorded at 240 Amu is the UD^+ cluster or that the UH_2^+ cluster becomes more distinct on more heavily hydrided samples. Though the SIMS provided definitive evidence for hydride formation, it could not differentiate whether the source of hydrogen was arising from (i) the water, through oxidation or (ii) the headspace gas, via diffusion. For the heavily corroded samples, where evidence for UH_3 formation was not definitive, we cannot rule out hydride formation. It may be that hydride formation was patchy (forming as isolated spots across the surface) or that the metal interface was buried to deeply for reliable results to be withdrawn via SIMS.

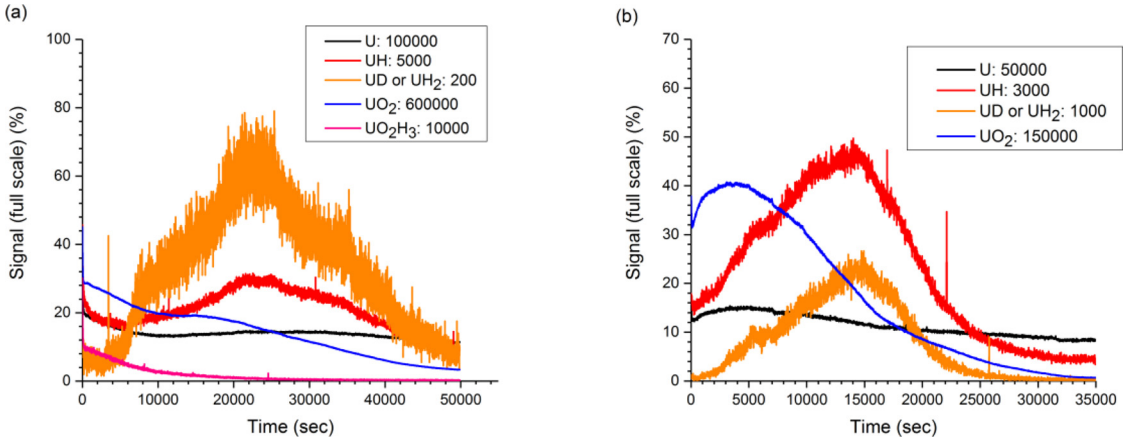

Fig. 5. Secondary ion mass spectrometry (SIMS) depth profiles for a) WD45 L and b) WD70 M sample. The analysis was performed with a Ga + primary ion beam, 25 keV voltage, 3 nA beam current, and 45° angle of incidence. Figures reproduced from [26].

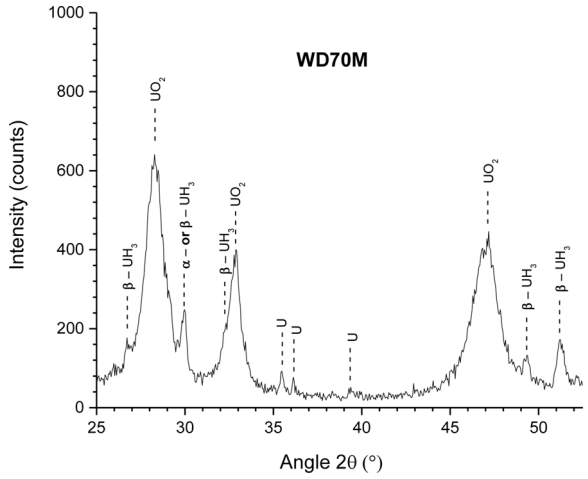

Fig. 6. Raw X-ray diffraction (XRD) spectra for WD70 M sample. The analysis were performed with a Cu-kα source at 8 keV, between 25 and 52.5° angle 2θ, 0.05 step and 5 s dwell time. Figure reproduced from [26].

Further analysis was required to establish whether hydride had formed on all samples, and if so, the contribution from UH_3 versus UD_3.

3.5. XRD analysis

X-ray diffraction analysis was used to investigate four of the corroded U samples: WD45 L, WD55 L, WD55H and WD70 M. Fig. 6 displays an example XRD spectrum recorded for sample WD70 M.

For samples WD55 L and WD55H (not shown here), the recorded diffraction profiles displayed only peaks associated with UO_2, no U metal or hydride peaks were observed, which was unsurprising given that the corrosion layer thickness far exceeded the sampling depth of the diffraction measurements. By comparison, the samples that could be characterised down to the metal surface (WD45 L and WD70 M), exhibited diffraction peaks that could be assigned to U, UO_2 and UH_3 (Figs. 6). For sample WD45 L (not displayed), the recorded uranium metal and hydride peaks had a very low intensity, while on WD70 M, which had significant corrosion layer spallation, these phases were much more clearly observed. For WD70 M, five UH_3 peaks were identified between 25–52.5 ° (2θ) (Fig. 6). XRD analysis therefore provided further confirmation for the existence of UH_3 on the corroded metal surfaces.

3.6. TPD - RGA analysis

Through thermal desorption with concurrent analysis of evolved gases, it was possible to provide further evidence for hydride formation as well as indicating the D:H ratio in the formed hydride. The thermal process followed here, was identical that conducted in [22]. The thermal cycle included the following stages:

Step 1: Temperature increase to $120 \leq T \leq 150$ °C for ~17 h under continual vacuum. This was considered sufficient time for each sample to release water, hydroxyl, CO, etc. entities from the near surface. The majority of physi- and chemisorbed waters (with associated phases) were considered to be removed by this initial thermal step.

Step 2: Temperature increase to ~220 °C under static vacuum. The working volume was then isolated from the vacuum pumping system to observe any subsequent pressure increase with heating and ensure that no other gases are released close to the lower temperature limit of UH_3 decomposition (~250 °C). In some cases, the gas profile showed further release, with gas analysis resolving a mixture of various gases. H_2, H_2O and OH^- were the dominating entities at this stage. In almost all cases at that stage, H_2 constituted ≤ 25% of the overall gas evolved. The temperature was kept constant until no further pressure increase was observed and the volume was then quickly evacuated to 1×10^{-7} mbar and then isolated again.

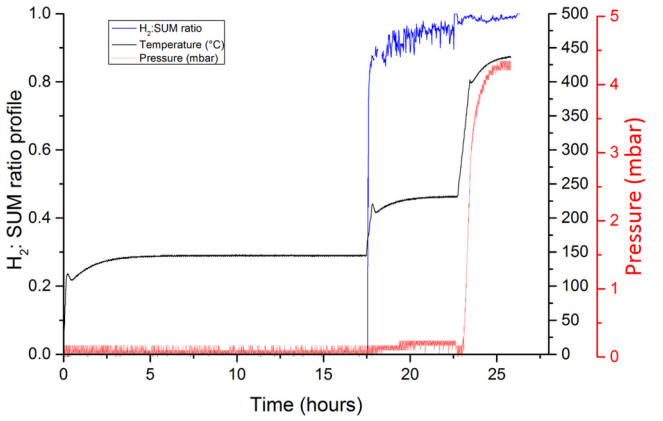

Fig. 7. Pressure vs. Temperature (P–T) plot from the thermal process (sample degassing) of WD55 M sample. The H2:SUM gas ratio (highlighted in blue) was also included in the plot. Pressure increase due to H2 generation is predominantly occurring when temperature is increased above 220 °C. Hydrogen generation at this stage is ascribed to UH3 decomposition. Figures reproduced from [26] (For interpretation of the references to colour in this figure legend, the reader is referred to the web version of this article).

Step 3: Temperature increase of the system to 360–440 °C.

The ratio of H_2 to the sum of evolved gases was calculated for each sample. RGA analysis was initially conducted for samples WD25 M, WD45 M, WD55 M, WD70 M and a reference non-reacted uranium sample. Apart from H_2, gases such as CH_4, H_2O, CO_2, N_2 were generated mainly during the first two stages of the thermal process, ascribed to degassing of surface water and organic contaminants associated with initial sample preparation. When the temperature was raised higher than ~220 - 250 °C (step 3 of thermal process), hydrogen was evolved in significant quantities and dominated the gas composition (> 99%) as shown in Fig. 7. Since hydrogen was almost exclusively generated in step 3 of the thermal process, it was decided not to analyse the gas composition arising from the remaining samples but to assume that it was exclusively H_2 for this stage of the TPD process. Pressure-temperature (P–T) profiles were generated for all remaining samples. Fig. 7 illustrates the P–T profile for sample WD55 M, exhibiting significant gas evolution in stage 3 of the TPD. This was the same behaviour for all samples, indicating that hydride had formed in some quantity on all the samples. Hydrogen evolved in earlier stages of the TPD, could either evolve from surface water decomposition [16] or hydride degradation (via oxidation) and accordingly these quantities were not included in our calculations. Subsequent derivations of the hydride mass formed on each sample must be considered conservative (Fig. 8).

It is significant to note that during TPD, no D_2 (mass peak 4) was evolved for any sample. This is a critical finding as it implies that no

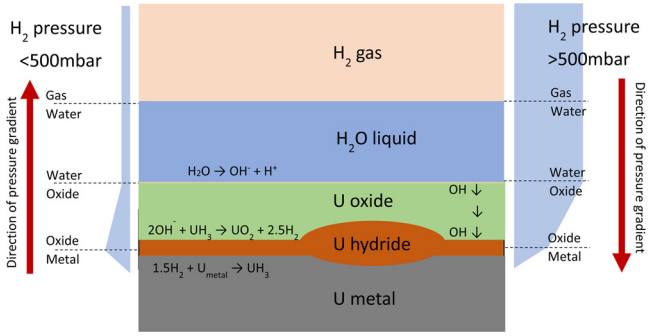

Fig. 8. Showing the conceptual movement and generation of hydrogen and hydride in the corrosion system.

Table 5
Bulk-hydride quantification for all reaction samples. The percentage ratio of UH_3 to overall solid reaction products was also calculated.

Sample	Reaction time (hours)	Working volume (cm^3)	Final T of decomposition (K)	Pressure increase due to UH_3 decomposition (mbar)	mmol of interlayer hydride (for avg. thickness of 5 nm)	mmol of bulk UH_3*	mmol of UO_2 (derived from Eq.1)	Percentage ratio of UH_3 to overall solid corrosion products (assuming only UO_2 and UH_3 are produced) (%)
WD25M	1091	108.4	675.2	12.84	5.34E-05	0.0147	0.0314	31.95
WD45L	1567.4	213.2	675.2	10.44	8.04E-05	0.0238	0.4175	5.39
WD45M	775	108.3	705.6	8.11	8.39E-05	0.0072	0.026	21.75
WD45H	1639	213.3	678.4	12.02	4.22E-05	0.0289	0.192	13.11
WD55L	1566	213.2	663.7	21.05	8.37E-05	0.0514	1.079	4.55
WD55M	1075	108.4	708.7	4.35	3.07E-05	0.0043	0.2682	1.58
WD55H	1092.3	213.2	667.9	11.63	8.15E-05	0.027	0.2878	8.59
WD70M	516	108.3	678.4	6.37	8.05E-05	0.0055	0.1226	4.27

* $moles_{final} = moles_{gas\ phase} - moles_{interlayer\ hydride} - moles_{stored\ UH3}$.

UD_3 formed within the system; only UH_3 had formed. By calibrating the volume of the cell where decomposition took place and knowing the final temperature of the system, the total pressure of gas (ascribed to H_2) could be converted to moles of H_2 through the ideal gas law equation. Thus, the amount of UH_3 in the sample could be quantified through the reverse of the reaction given in Eq. 2. However, as explained already in [22], there were three types of UH_3 decomposing between 225–450 °C: (a) primordial UH_3, formed through the initial metal fabrication process; (b) interfacial hydride, forming as a very thin layer at the metal-oxide interface during water corrosion; and (c) bulk-hydride formation through water corrosion [22]. Bulk-UH_3 which presents the most 'harmful' type of hydride, was the one targeted to be quantified. To subtract the contribution of 'pre-existing' hydride, multiple reference uranium samples (polished and non-reacted) underwent the same TPD process and the amount of hydrogen generated was related to the mass of the sample. This correction was then applied to all the corroded samples to provide the corrected quantity of bulk-UH_3 in each system (Table 5).

High relative bulk-hydride percentages were derived for samples WD25 M and WD45 M, calculated as 31.95% and 21.75% of the total corrosion product, respectively. This correlates with the very low reaction rate regimes recorded from H_2 gas evolution indicating that a higher quantity of oxidation-formed H^+ was reacting to form UH_3 (through Eq. 2) instead of diffusing into the headspace as H_2. Similarly to the binary system previously reported [22], the percentage of bulk-hydride present in the solid reaction products decreased with increasing reaction temperature, even though the absolute amount of UH_3 in the higher temperature reacting samples was greater.

Reaction time could potentially have had an effect on the percentage of UH_3 on samples reacting at 45 °C, with WD45 M showing a significantly higher percentage for a shorter reaction time. One very significant finding from the analysis of samples reacting at 45 and 55 °C was that the UH_3 percentage was significantly lower on the samples with initial headspace pressures below the 'threshold pressure', in comparison to those above the threshold pressure. The argument that this could be solely an effect of the more extended reaction time (and not also the threshold pressure), would not hold since samples WD45 L and WD45H were reacted for very similar time periods.

4. Discussion and conclusions

The results clearly indicate that bulk hydride formation had occurred on all the reacted U samples, determined both directly and indirectly. As displayed in Table 5, it was found that the amount of UH_3 as a percentage of the total mass of corrosion product for each sample was related to (a) the reaction temperature, (b) the reaction time period and (c) the initial headspace D_2 pressure in the reaction system. Higher reaction temperatures resulted in a smaller proportion of the corrosion product being UH_3, even though the absolute mass of UH_3 generated was greater. This was attributable to the enhanced oxidation kinetics at higher temperatures, leading to more substantial sample oxidation over a given period for lower reaction temperatures. The duration of corrosion was also found to somewhat affect the proportion of UH_3 in the corrosion products. Extended reaction periods resulted in a smaller proportion of UH_3, especially in the higher temperature regimes (e.g. samples WD55 L and WD55H – Table 5). From physical observation of the reacted samples, it was inferred that higher reaction temperatures lead to thicker (due to faster kinetics), but more poorly consolidated and adhered oxide on the surface. This porous structure would enable water to directly react with the UH_3 buried under the oxide, converting it to UO_2 (Eq. 3). The same effects of temperature and time were observed for previous corrosion experiments conducted on the binary uranium-water system [22].

$$2\boldsymbol{UH_3} + 4\boldsymbol{H_2O} \rightarrow 2\boldsymbol{UO_2} + 7\boldsymbol{H_2} \quad (3)$$

In [22] a headspace 'threshold pressure' was suggested, above which the rate of H_2 liberation into the headspace volume from U corrosion was decreased. It was suggested that this marked rate change indicated the onset of bulk-UH_3 formation in the system. This pressure was found to be in the 0.5 bar range. Here, for the 45 and 55 °C reaction, the D_2 headspace pressures were chosen deliberately below (denoted as L), at (denoted as M) and above (denoted as H) this 'threshold pressure' to accelerate the onset of UH_3 formation to different extents. From Table 6, it was found that the proportion of UH_3 in the arising corrosion product was higher for the samples with starting D_2 pressures above this previously identified 'threshold pressure'. This effectively verified the proposition made in [22] with regards to facilitation of UH_3 formation above this 'threshold pressure'.

A further purpose of the present experiments was to validate whether the previously observed hydride formation was attributable to (i) hydrogen gas diffusing through the water from the headspace to react at the metal surface or (ii) hydrogen derived from splitting of water or hydroxyl ions at the metal surface concurrent with oxide formation (Eq. 1).

Most significant in verifying the contributor to hydride formation was the TPD-RGA degassing analysis of the corroded samples. The results clearly indicated that the hydrogen attributable to hydride formation was chemically derived from the water and not the headspace gas, because no significant detectable D_2 was recorded during hydride decomposition. In future work, it would be logical to test this attribution by reversing the hydrogen isotopes in the experimental system and using heavy water (D_2O) with a cover gas of hydrogen (H_2).

This is a significant observation and indicates that the mechanism for hydride formation involves the headspace gas performing the role of

reversing or balancing the hydrogen pressure gradient in the corrosion system. At below the 500-mbar threshold headspace pressure it is inferred that the highest hydrogen pressure in the system is at the uranium oxide-metal interface. Hence any evolved hydrogen (from corrosion) diffuses out from the interface through the oxide and cover water, into the lower-pressure headspace. At above 500 mbar, the pressure gradient starts to tip in the opposite direction, causing hydrogen released by oxidative corrosion to persist in greater quantities at the uranium surface causing hydride formation.

This is of course an oversimplification of the processes likely occurring. Initially it is more thermodynamically favourable for water to provide the hydrogen source for hydride formation, as water was the specie immediately contacting the outermost sample surface. However, it would be inevitable that deuterium from the headspace would subsequently dissolve into the reaction water and even reach the oxide surface and contribute to hydride formation, as evidenced by our SIMS analyses. However, our TPD analysis indicates that deuterium, whilst it may be present in the hydride, was an insignificant contributor. This behaviour may partly be explained by the work of Tiferet et al. [24] whose study showed that chemisorption of hydrogen onto uranium in the presence of water vapour is very limited, due to domination of surface adsorption sites by dissociated water.

From the findings of this work, corresponding with [22], the reaction of uranium in liquid water with a sealed headspace D_2 overpressure ($U + H_2O + D_2$) may be described by the following steps:

1) Initial oxidation of the sample by water. At this stage oxide thickening occurs on the sample surface, combined with H^+ ion formation at the metal-oxide interface, liberated during partial dissociation of water ($H^+ - OH^-$) at the oxide surface and oxide formation through anionic movement of OH^- through the oxide lattice (prevalent diffusing entity). Through that mechanism [9] the H^+ ions either couple with each other to form molecular hydrogen and diffuse to the outer surface of the sample or remain at the metal-oxide interface where they build up in pressure to eventually react with the metal and form UH_3. At the start of the experiment, before the D_2 could achieve an equilibrium saturation with the water, H^+ liberated by U oxidation is assumed to have diffused outwards into the water and hydride formation would not have occurred. Hydride formation cannot be excluded at this step of the process, but it considered less likely as the hydrogen pressure at the metal-oxide interface is likely higher than in the water irrespective of the headspace gas pressure.
2) Subsequently, with continued corrosion where a critical headspace pressure is reached, referred to as the 'threshold pressure', the generated H^+ from U oxidation by water will begin to contribute to bulk-UH_3 formation (alongside continued oxide formation), with less H^+ being contributed to the gas phase. This was manifested by a decrease in the rate of H_2 gas evolution in the cell headspace. This 'threshold pressure' was calculated in [22] to be ˜500 mbar, including the coexisting water vapour pressure. Our experiments initiated with headspace D_2 below, at and over the 'threshold pressure', have confirmed this threshold switch in corrosion behaviour. It is important to note that UH_3 formation could occur prior to the 'threshold pressure' being achieved. However, above this pressure, H_2 gas evolution deceleration will facilitate if not accelerate the phenomenon of UH_3 formation, since the concentration of H^+ at the metal-oxide interface will be higher because the accumulated headspace gas essentially balances (or reverses) the hydrogen pressure across the system.
3) Over prolonged periods of corrosion (> 100's hours) the accumulated oxide which initially protects the underlying hydride that is forming, becomes more poorly protective due to cracking and spallation. Exposed UH_3 will readily react with water to form UO_2, releasing H_2 as a by-product. This was manifested in our experiments as a switch to a higher gas generation rate (Fig. 2-3rd reaction regime). By comparing the amount of UH_3 produced relative to the amount of UO_2 for each system it was found that longer reaction periods resulted in proportionally smaller amount of UH_3. This was expected as the water will readily oxidise the UH_3 in addition to the metal.

The current study has revealed an interesting set of dynamics for the $U + H_2O + H_2$ corrosion system, using D_2 as a tracking isotope. The observation of a threshold pressure for 'switching on' bulk-UH_3 is significant and it is not currently understood if this observed influence on corrosion exerted by exceeding the 500 mbar H_2 threshold pressure in the headspace, will be reproduced by other gas mixtures e.g. a 1 bar 80:20 N_2-H_2 mixture or a 1 bar 4:18:78 H_2-O_2-N_2 mixture analogous to the threshold explosive concentration of hydrogen in air. Understanding this behaviour is considered important for predicting the corrosion state of uranium in existing storage facilities and for 'inerting' activities that are planned during legacy material retrievals at Sellafield. This will form the basis for ongoing experiments.

To summarize, the low temperature corrosion reaction of uranium with liquid water under a D_2 headspace overpressure was investigated under immersed conditions with a sealed volume. Nine samples were examined at four different temperatures (25, 45, 55 and 70 °C), and by varying reaction time and headspace overpressure. The rate of the reaction was derived from monitoring progressive pressure changes in the reaction cell (ascribed to H_2 generation from oxidation). Post-reaction examination of the corroded uranium surfaces was conducted using FIB, SIMS and XRD analysis. Commensurate pH measurements of the residual reaction waters were also conducted to examine gas dissolution. Finally, the samples were degassed using a three-step thermal desorption-decomposition process, to verify any UH_3 formation and determine the mass formed in each system. Residual gas analysis (RGA) of the desorbed gases was used to determine the composition of the evolved gases.

From the analyses, it was concluded that:

i Bulk UH_3 forms at the metal-oxide interface, on the majority of the samples. This was established through SIMS, XRD and TPD analysis.
ii UH_3 as a proportion of the overall solid reaction products on each sample (UH_3 and UO_2) was derived for each system. It was found that lower temperature reaction conditions yielded higher proportions of UH_3 in the arising corrosion products. However, the absolute UH_3 quantities were higher for the samples reacted at higher temperatures. It was observed that for higher temperatures, the formed oxide is thicker but more poorly adhered to the surface, with significant delamination and spallation. Alongside enhanced oxidation kinetics at higher temperatures, this facilitates water contacting and oxidizing bulk hydride, leading to proportional reduction of the UH_3 within the system.
iii Extended reaction periods resulted in smaller proportions of UH_3 in the overall mass of corrosion products, especially in the higher temperature regimes (samples WD55 L and WD55H – Table 5).
iv By using D_2 in the headspace at pressures below, at and above the 'threshold pressure' (˜500 mbar) suggested by [22] a switch in the rate of gas liberation from U water corrosion was observed. Through the use of isotopic labelling it was established that hydrogen generated through oxidation of U by water, and **not** D_2 gas migration from the headspace, was responsible for hydride formation.

Acknowledgements

The authors would like to thank the Engineering and Physical Sciences Research Council (EPSRC) and Sellafield Ltd for funding this project as part of 42-month PhD research studentship (Ref: 1338575), at the Interface Analysis Centre (IAC), School of Physics, University of Bristol. We would also like to thank Mr John Jowsey and Dr Anna Adamska from the Sellafield Centre for Expertise in Uranium and

Reactive Metals (URM) for contextual guidance and technical input.

References

[1] Nuclear decommissioning authority (NDA), Radioactive Wastes in the UK: a Summary of the 2016 Inventory, Nuclear decommissioning authority (NDA), Cumbria, 2016.
[2] Pile Fuel Storage Pond, Sellafield Ltd, Cumbria, 2013www.sellafieldsites.com.
[3] C. Ablitzer, F. Le Guyadec, J. Raynal, X. Génin, A. Duhart-Barone, Influence of superficial oxidation on the pyrophoric behaviour of uranium hydride and uranium powders in air, J. Nucl. Mater. 432 (2013) 135–145.
[4] F. Le Guyadec, X. Génin, J. Bayle, O. Dugne, A. Duhart-Barone, C. Ablitzer, Pyrophoric behaviour of uranium hydride and uranium powders, J. Nucl. Mater. 396 (2010) 294–302.
[5] J. Frank, A. Roebuck, Crevice Corrosion of Uranium and Uranium Alloys, (ANL -5380), Argonne National Laboratory, Lemont, Illinois, 1955.
[6] J. Draley, W. Ruther, Some unusual effects of hydrogen in corrosion reactions, J. Electrochem. Soc. 104 (1957) 329–333.
[7] B. Hopkinson, Kinetics of the uranium-steam reaction, J. Electrochem. Soc. 106 (1959) 102–106.
[8] T. Kondo, E. Verink, F. Beck, M. Fontana, Gas chromatographic and gravimetric studies of uranium oxidation mechanism, Corrosion 20 (1964) 314t–320t.
[9] M.M. Baker, L. Less, S. Orman, Uranium + water reaction. Part 1.- Kinetics, products and mechanism, Trans. Faraday Soc. 62 (1966) 2513–2524.
[10] T. Kondo, F. Beck, M. Fontana, A Gas chromatographic study on the kinetics of uranium oxidation in moist environments, Corrosion 30 (1974) 330–341.
[11] M. Bennett, B. Myatt, D. Silvester, J. Antill, The oxidation behaviour of uranium in air at 50-300° C, J. Nucl. Mater. 57 (1975) 221–236.
[12] K. Winer, C. Colmenares, R. Smith, F. Wooten, Interaction of water vapour with clean and oxygen-covered ur anium surfaces, Surf. Sci. 183 (1987) 67–99.
[13] S.C. Marschman, T. Pyecha, J. Abrefah, Metallographic Examination of Damaged N Reactor Spent Nuclear Fuel Element SFEC5, 4378, Pacific Northwest Laboratory, Richland, WA (United States), 1997.
[14] J. Abrefah, R.L. Sell, Oxidation of K-west Basin Spent Nuclear Fuel in Moist Helium Atmosphere, (No. PNNL-12167), Pacific Northwest National Laboratory, Richland, WA (US), 1999.
[15] T.C. Totemeier, R.G. Pahl, S.M. Frank, Oxidation kinetics of hydride-bearing uranium metal corrosion products, J. Nucl. Mater. 265 (1999) 308–320.
[16] A. Danon, J. Koresh, M. Mintz, Temperature programmed desorption characterization of oxidized uranium surfaces: relation to some gas-uranium reactions, Langmuir 15 (1999) 5913–5920.
[17] C.H. Delegard, A.J. Schmidt, Uranium Metal Reaction Behaviour in Water, Sludge, and Grout Matrices, (No. PNNL-17815), Pacific Northwest National Laboratory, 2008.
[18] J. Waber, A Review of the Corrosion Behaviour of Uranium, Los Alamos Scientific Laboratory, New Mexico, 1956.
[19] C. Colmenares, R. Howell, T. McCreary, Oxidation of Uranium Studied by Gravimetric and Positron Annihilation Techniques, (No. UCRL-85549; CONF-810332-2), Lawrence Livermore National Laboratory, CA (USA), 1981.
[20] J.M. Haschke, Reactions of Plutonium and Uranium With Water: Kinetics and Potential Hazards, (No. LA–13069-MS), Los Alamos National Laboratory, 1995.
[21] M. Kaminski, Batch Tests with unirradiated uranium metal fuel program report, (No. ANL-01/33), Argonne National Laboratory, Illinois (USA, 2002.
[22] A. Banos, K.R. Hallam, T. Scott, Corrosion of Uranium in Liquid Water Under Vacuum Contained Conditions. The Initial Binary U + $H_2O_{(l)}$ system., Under Submission, (2018).
[23] M.M. Baker, L. Less, S. Orman, Uranium + water reaction. Part 2. - Effect of oxygen and other gases, Trans. Faraday Soc. 62 (1966) 2525–2530.
[24] E. Tiferet, M. Mintz, I. Jacob, N. Shamir, Inhibition of hydrogen chemisorption on uranium surfaces by traces of water vapour, Surf. Sci. 601 (2007) 4925–4930.
[25] E. Tiferet, M. Mintz, S. Zalkind, I. Jacob, N. Shamir, Heat treatment effects on the surface chemisorption behaviour of strained uranium: The H_2O/U reaction, J. Alloys. Compd. 444 (2007) 177–183.
[26] A. Banos, Investigation of Uranium Corrosion Under Mixed Water-hydrogen Environments, PhD thesis University of Bristol, Bristol, 2017.
[27] A. Banos, C.P. Jones, T.B. Scott, The effect of work-hardening and thermal annealing on the early stages of the uranium-hydrogen corrosion reaction, Corros. Sci. 131 (2018) 147–155.
[28] A. Banos, C. Stitt, T. Scott, The effect of sample preparation on uranium hydriding, Corros. Sci. 113 (2016) 91–103.
[29] A. Banos, T.B. Scott, Statistical analysis of UH_3 initiation using electron backscattered diffraction (EBSD), Solid State Ion. 296 (2016) 137–145.
[30] E. Wilhelm, R. Battino, R.J. Wilcock, Low-pressure solubility of gases in liquid water, Chem. Rev. 77 (1977) 219–262.
[31] T.C. Totemeier, A Review of the Corrosion and Pyrophoricity Behaviour of Uranium and Plutonium, Government Research Announcements and Index, (1995) USA 45.
[32] N. Harker, The Corrosion of Uranium in Sealed Environments Containing Oxygen and Water Vapour, PhD thesis University of Bristol, Bristol, 2012.